ELSEVIER

Polymer 43 (2002) 5219–5226

polymer

www.elsevier.com/locate/polymer

Deformation studies of single rigid-rod polymer-based fibres. Part 1. Determination of crystal modulus

M.A. Montes-Morán[a], R.J. Davies[a], C. Riekel[b], R.J. Young[a,*]

[a]*Manchester Material Science Centre, Polymer Science and Technology Group, University of Manchester and UMIST, Grosvenor Street, Manchester M1 7HS, UK*

[b]*European Synchrotron Radiation Facility, B.P. 220, F-38043 Grenoble Cedex, France*

Received 28 February 2002; received in revised form 30 May 2002; accepted 31 May 2002

Abstract

This series of papers covers several aspects related to the influence of external stresses on the crystalline microstructure of rigid-rod polymer-based fibres. For the study, the main three fibres of this type have been selected, namely poly(*p*-phenylenebenzobisoxazole) (PBO fibres), poly(*p*-phenylenebenzobisthiazole) (PBT or PBZT fibres) and the novel poly{2,6-diimidazo[4,5-*b*:4′-5′-*e*]pyridinylene-1,4(2,5-dihydroxy)phenylene} (PIPD or M5 fibres). Synchrotron radiation was employed to record high-quality wide-angle X-ray scattering patterns from single fibres. The present paper deals mainly with the evaluation of lattice strain along the fibre axis (*c*-)direction. Crystal moduli of the different fibres were calculated from the variation with stress of the lattice strain determined from the shift of the major meridional (00*l*) reflections. This procedure rendered values of approximately 440 GPa for the crystal modulus of PIPD and PBO fibres, and 350 GPa for the PBT one. The difference between these two values was explained in terms of specific molecular conformation of the monomers in the unit cell. Discrepancies between the crystal and macroscopic (calculated from tensile tests) moduli are due to imperfections generated during the manufacture of the fibres.

Keywords: Poly{2,6-diimidazo[4,5-*b*:4′-5′-*e*]pyridinylene-1,4(2,5-dihydroxy)phenylene} fibres; Poly(*p*-phenylenebenzobisthiazole) fibres; Poly(*p*-phenylenebenzobisoxazole)fibres

1. Introduction

The US Air Force sponsored and participated in a specific polymer programme for the development of new structural materials with high specific strength and modulus, more than 20 years ago [1,2]. Various of the so-called rigid-rod polymers were then investigated, particularly poly(*p*-phenylenebenzobisoxazole) or PBO and poly(*p*-phenylenebenzobisthiazole) or PBT:

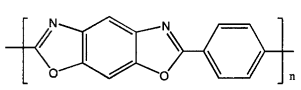

PBO

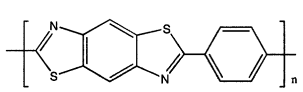

PBT

Fibres obtained from these rigid-rod polymers exhibit remarkable strength and modulus, cut and abrasion resistance, as well as long-term retention of their properties at relatively high temperatures [3,4]. Their compressive performance, however, is rather poor since fibre behaviour in compression is determined strongly by inter-chain interactions [5,6]. To overcome this drawback, a novel rigid-rod polymer-based fibre was developed in the former Akzo Nobel Central Research at the end of last century, the poly{2,6-diimidazo[4,5-*b*:4′-5′-*e*]pyridinylene-1,4(2,5-dihydroxy)phenylene} or PIPD (also known as 'M5') [6–9]:

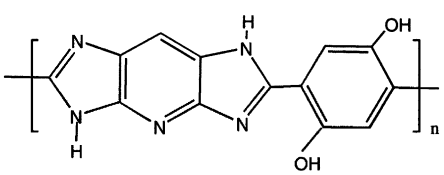

PIPD

This new polymer combines essential features of a rigid skeleton (i.e. stiffness, flame resistance) with strong hydrogen bonds between polymer chains similar to those existing in aramid fibres. As a result, the compressive

* Corresponding author. Tel.: +44-161-200-3551; fax: +44-161-200-8877.

E-mail address: robert.young@umist.ac.uk (R.J. Young).

0032-3861/01/$ - see front matter
PII: S0032-3861(02)00345-2

strength of PIPD fibres is almost an order of magnitude higher than the observed for other rigid-rod polymer-based fibres [8,9].

One common attribute of all rigid-rod polymer-based fibres is its high degree of molecular orientation. Manufacturing processes of these fibres include normally a dry-jet wet spinning step, where the rigid-rod molecules are extruded through a spinnerette [4,9]. Shearing forces thus tend to align the molecular chains along the fibre axis, bringing about a highly crystalline microstructure. Heat treatment under tension of these as spun fibres has demonstrated to improve this crystallinity [2]. Nevertheless, rigid-rod polymer-based fibres are very suitable to be characterised by means of diffraction techniques. X-ray diffraction (XRD), for example, has been employed widely to characterise the morphology (i.e. microstructure, type of unit cell) of this type of fibres. Atomic positions in the unit cells of PBO, PBT and PIPD fibres have been measured accurately by means of wide angle X-ray scattering (WAXS) [2,7].

WAXD was also employed to evaluate the lattice strain of highly crystalline polymeric fibres (PBO, PBT and PPTA), following a method based loosely on theory proposed by Dulmage and Contois in 1958 [10]. In these experiments, a bundle of fibres are submitted to a macroscopic stress and the microscopic deformation of the unit cell is followed by XRD, hence allowing the calculation of the so-called crystal modulus. Lenhert and Adams [11] were the first to complete successfully such an experiment for PBO and PBT using fibre bundles in 1988, although more recently other research groups have replicated their results [12–14]. The crystal modulus value is, in principle, an intrinsic property of a given rigid-rod polymer-based fibre, since it corresponds to the stiffness of its polymer backbone. It is thus considered the ultimate fibre (macroscopic) modulus, the value that would be reached if imperfections or defects were eventually eliminated.

This article constitutes the first in a series of papers that examines single-fibre deformation of PBO, PBT and PIPD fibres by means of synchrotron XRD. The experiments entailed the use of beam size of a few micrometers, which was scanned across the fibre [15–18]. The synchrotron radiation is powerful enough to allow the recording of high-quality WAXS patterns from single-fibres. From the analysis of all three rigid-rod polymer-based fibre varieties (PIPD, PBO and PBT), conclusions could be drawn as to the influence of a particular molecular conformation or processing differences on the final properties of the fibres produced. The relevance of the results also points in the same direction, since they might help to design new rigid-rod polymers or to explore new routes of manufacturing that could improve the mechanical properties of the existing fibres. This first paper of the series is concerned primarily with determination and comparison of single-fibre crystal modulus values for three fibre varieties, with future papers examining other elements from the diffraction patterns such as crystallite orientation, and fibre skin–core morphology.

2. Experimental

2.1. Materials characterisation

Three different types of rigid-rod polymer-based fibres were characterised. The PIPD fibres, metallic blue in colour, were supplied by Akzo Nobel Central Research, The Netherlands. The polymer was synthesised by Akzo Nobel Research and the fibres were spun from liquid crystalline solutions. They were also heat treated after spinning to improve the mechanical properties.

The ‘as-spun’, straw coloured, PBT fibres were supplied by the Materials Laboratory of the Wright-Patterson Air Force Base, OH, USA. Fibres were prepared from a liquid crystalline solution in a concentrated acid. No further heat treatment was given to these as spun fibres.

As spun PBO fibres supplied by Toyobo, Japan, were also characterised. They are fibres available commercially under the trade name Zylon^{TM}. Details of their fabrication can be found elsewhere [13].

The mechanical properties of the specimens were measured using an Instron 1121 universal testing machine using a 1N load cell and Workbench data logging software. All testing was carried out in a standard atmosphere at a cross-head speed off 2 mm min^{-1}, using samples that had been pre-conditioned for a minimum of 24 h. The samples were prepared within cardboard windows, and fixed in place using cold-curing epoxy resin.

Previous studies have shown that both Young’s modulus and tensile strength of these type of fibres are gauge length sensitive [3,9]. As a result, testing of each variety of rigid-rod polymer-based fibres was undertaken using three different gauge lengths, namely 20, 50 and 100 mm. At least 10 samples were tested at each gauge length. The modulus results were extrapolated to infinite gauge length in order to eliminate the influence of end effects, and strength results extrapolated to zero gauge length to account for the influence of critical flaws.

A Philips series XL-30 Field Emission Gun Scanning Electron Microscope was used to determine accurately the diameter of the fibres used in this work. The diameter measurements were made using three different levels of magnification, all of which had been previously calibrated using a graticule. At least 10 fibres were then selected at random for each variety of rigid-rod polymer-based fibre and the average and standard deviation calculated for each.

2.2. X-ray diffraction

XRD characterisation of the fibres was carried out at the European Synchrotron Radiation Facility (ESRF) on beamline ID13 (micro-focus beamline) at an X-ray wavelength of

Table 1
Dimensions and mechanical properties of the rigid-rod polymer fibres studied

	Fibre diameter (μm)	Strength (GPa)	Modulus (GPa)	Crystal modulus[a] (GPa)
PIPD	11.5 (±0.8)	3.7 (±0.3)	265 (±18)	320–390
PBT	13.3 (±0.9)	2.3 (±0.4)	205 (±21)	350
PBO	12.3 (±1.1)	4.8 (±0.6)	180 (±10)	390

[a] The PIPD data were estimated from mechanical testing extrapolating data for perfect crystal orientation [8]. The PBT and PBO data were determined by XRD during deformation of fibre bundles [11].

0.0948 nm. The beamline was configured with the beam stopped down to an approximately 2 μm diameter spot size and a MARCCD detector [15,16]. The specimen-to-film distance was calculated using an Al_2O_3 sample and was found to be approximately 68 mm. The fibres were loaded using a single-fibre stretching rig that was designed to fit to the $x-y-z$ drive plate of the beamline stage. The deformation rig is based on a piezo stretching mechanism, and the load measured using an incorporated load cell. The gauge length between the mounting plates of the rig was 3.8 mm with a full deflection of 280 μm. Samples were glued (cyanoacrylate adhesive) directly to the mounting plates, and cured in situ prior to collection of data. Both the piezo mechanism and the recording of the load cell data were monitored from within the control cabin. A diffraction pattern (15 s of scan time) was obtained from the centre of the fibre sample at increasing levels of loading, until either fibre fracture or de-bonding from the adhesive took place. This procedure was performed for all the fibres under study.

All data analysis (background correction, radial and azimuthal integration, profile fitting) was carried out using the FIT2D software application version 10.95 [19,20]. Additional details to calculate the crystal modulus are given elsewhere [13].

3. Results and discussion

3.1. Tensile testing

The fibre diameters necessary for Young's modulus and tensile strength calculations were obtained from scanning electron micrographs with the microscope magnification carefully calibrated using a grid of known dimensions. Measurements of at least 20 single filaments were employed to calculate the average diameter of each rigid-rod polymer-based fibres. These average values are collected in Table 1.

Fig. 1 shows typical stress–strain curves for PIPD, PBT and PBO fibres under study, at 50 mm gauge length. As expected, PIPD fibre exhibits the higher modulus, given that it is the only heat-treated fibre under study. As spun PBO and PBT fibres, on the other hand, show similar values of Young's modulus in the initial part of the plot. The PBO fibre has the highest tensile strength (~5 GPa) along with fracture strain values of up to 3%. The tensile behaviour of the as-spun PBT fibre is rather unique when compared to the other two rigid-rod polymer-based fibres under study. It can be clearly seen from Fig. 1, a prominent deviation from linearity at strain values of about 1%. This yielding process, which is absent in the stress–strain curves of heat-treated PBT fibres [3], may take place through a mechanism such as molecular translation along the stressing direction.

The dependence of fibre tensile modulus and strength with testing gauge length is shown in Fig. 2. Values of both Young's modulus and tensile strength decrease with gauge length [3,9]. The rise of modulus at shorter gauge lengths is due to the so-called end effects, whereas the decrease of fibre strength at higher gauge lengths is explained in terms of critical flaw concept (i.e. the fibre strength is controlled by the effect of impurities and inhomogeneities). Thus, extrapolation of Young's modulus and tensile strength to infinite and zero gauge length, respectively, will render the corrected or true values for these magnitudes (Fig. 2). Results obtained from extrapolations are also given in Table 1. In general terms, values of Young's modulus and tensile strength of the fibres under study follow the trends just discussed when describing the stress–strain curves (Fig. 1).

3.2. XRD of undeformed fibres

Fig. 3 shows the unloaded (top) and loaded (bottom) single-fibre diffraction patterns of PIPD, PBT and PBO fibres collected at the ESRF. The strong equatorial reflections and multiple meridional reflections indicate a high degree of crystallite orientation along the fibre axis and

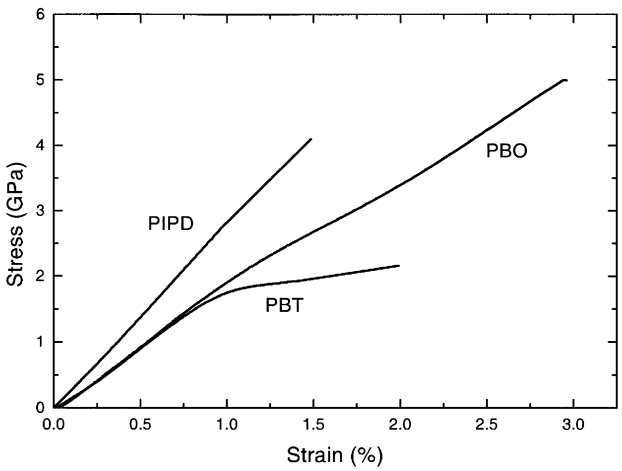

Fig. 1. Tensile stress–strain curves for single PIPD, PBT and PBO fibres.

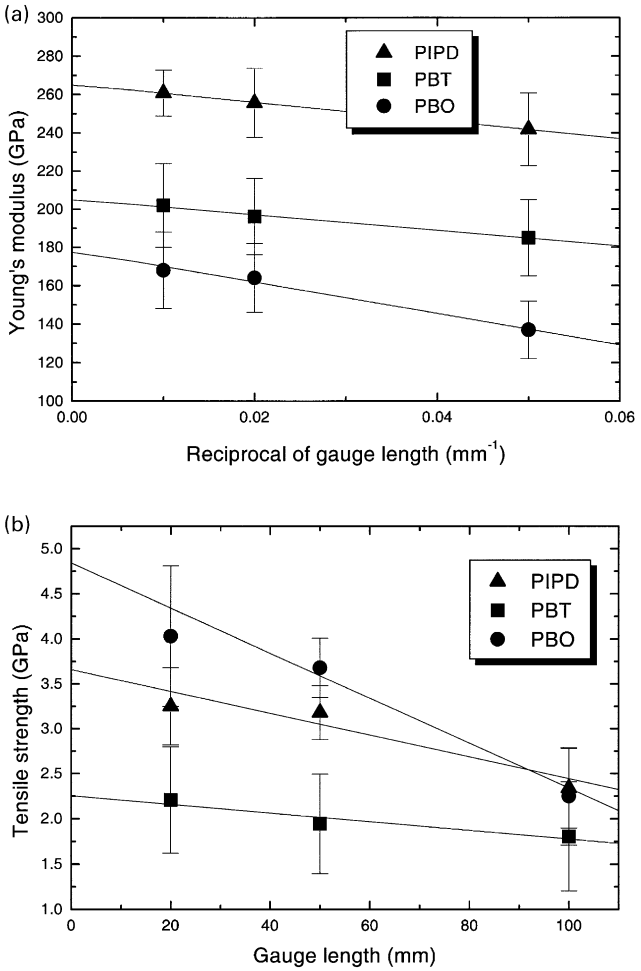

Fig. 2. Variation of (a) Young's modulus and (b) tensile strength with gauge length for single PIPD, PBT and PBO fibres.

suggest a good lateral packing of the stiff-molecules within the fibre, for all the fibres under study. However, the absence of off-axis reflections reveals the poor three-dimensional ordering of the polymer chains within the fibres. The parameters of the unit cell and indexes of the reflections observed for PIPD, PBT and PBO fibres have been determined previously by other researchers [7,11]. Regarding the meridional reflections, it is found that all the fibres under study show relatively similar diffraction patterns, with the (003), (005) and (006) reflections being the strongest ones. The intensity of the (003) and, in general, of the low angle ($l < 5$) meridional reflections is much lower for the PIPD fibre than for both PBO and PBT, thus indicating that the *ab*-plane of the PIPD unit cell is not perpendicular to the *c*-axis [7]. On the other hand, only the PBT XRD pattern exhibits the (002) reflection. The lack of the (002) reflection in PBO diffraction patterns is usually related to a $\pm 1/4$ *c*-axis translation of the molecular chains along the (100) direction [21,22].

Another common feature to rigid-rod polymer-based fibres is the existence of streaking in the meridional lines, which has been attributed to translational disorder in

Table 2
FWHM data of the XRD Bragg main reflections

	XRD reflections (mm)					
	(003)	(005)	(006)	(200)	(h10)[a]	($\bar{2}$10)
PIPD	0.6	1.1	1.8	1.7	2.1	
PBT	0.6	1.0	1.8	2.8	6.7	
PBO	0.7	1.1	1.8	1.8	3.0	1.4

[a] $h = 1$ for PIPD; $h = 0$ for PBO and PBT.

molecular packing along the fibre (*c*-)axis [3,23]. The amount of this molecular disorder, as measured by the full width at half maximum height (FWHM) of the meridional reflections (Table 2), is effectively the same for all the fibres. In other words, the distribution of *c*-spacings is the same regardless of the rigid-rod polymer-based fibre characterised in the present work. This result is rather surprising, especially in the case of the PIPD fibre. As mentioned earlier, this fibre was the only one submitted to a heat treatment by the manufacturer. It would be then expected a higher degree of chain orientation in the PIPD fibre compared to that of the as spun PBO or PBT fibres. Furthermore, a significant decrease of the FWHM values of the meridional reflections after heat treatment of as spun PBO fibres has been reported recently [13]. Nevertheless, the crystallinity of the rigid-rod polymer-based fibres is still far less developed than that of PPTA fibres [3,24].

Fig. 4 shows the radial profiles along the equatorial direction corresponding to the XRD patterns of PIPD, PBO and PBT unloaded fibres (Fig. 3 top). The relative position of the two main equatorial reflections of PIPD fibres gives an indication of their microstructure. Klop and Lammers [7] have shown that the (200) reflection of as spun PIPD fibres shifts to larger angles with heating, due to a dehydration process. These authors found a continuous variation from 8.38 Å, corresponding to the reflection of the two-dimensionally ordered hydrate structure of the as spun PIPD fibre, to 5.98 Å for the final dehydrated structure of the heat treated (500 °C) PIPD fibre. The (200) reflection of the PIPD sample analysed in the present work is located at 6.22 Å, thus being slightly (but significantly) larger than that of the fibre treated at 500 °C, according to Klop and Lammers [7]. This would also result in a less perfect crystal structure, which supports the absence of off-axis reflections in the PIPD X-ray diffractograms (Fig. 3), as well as the relatively high *c*-spacing distribution discussed earlier (Table 2). Obviously, it cannot be assured here that the heat treatment at 500 °C will reduce the FWHM values of the (00*l*) reflections.

It is also interesting to compare the equatorial reflections of PBT and PBO fibres. Although both specimens are as spun fibres, their equatorial profiles are remarkably different (Fig. 4). The two main equatorial peaks of the PBT fibre are not well defined, showing a continuous scattering between the (200) and (010) reflections. These two peaks come into

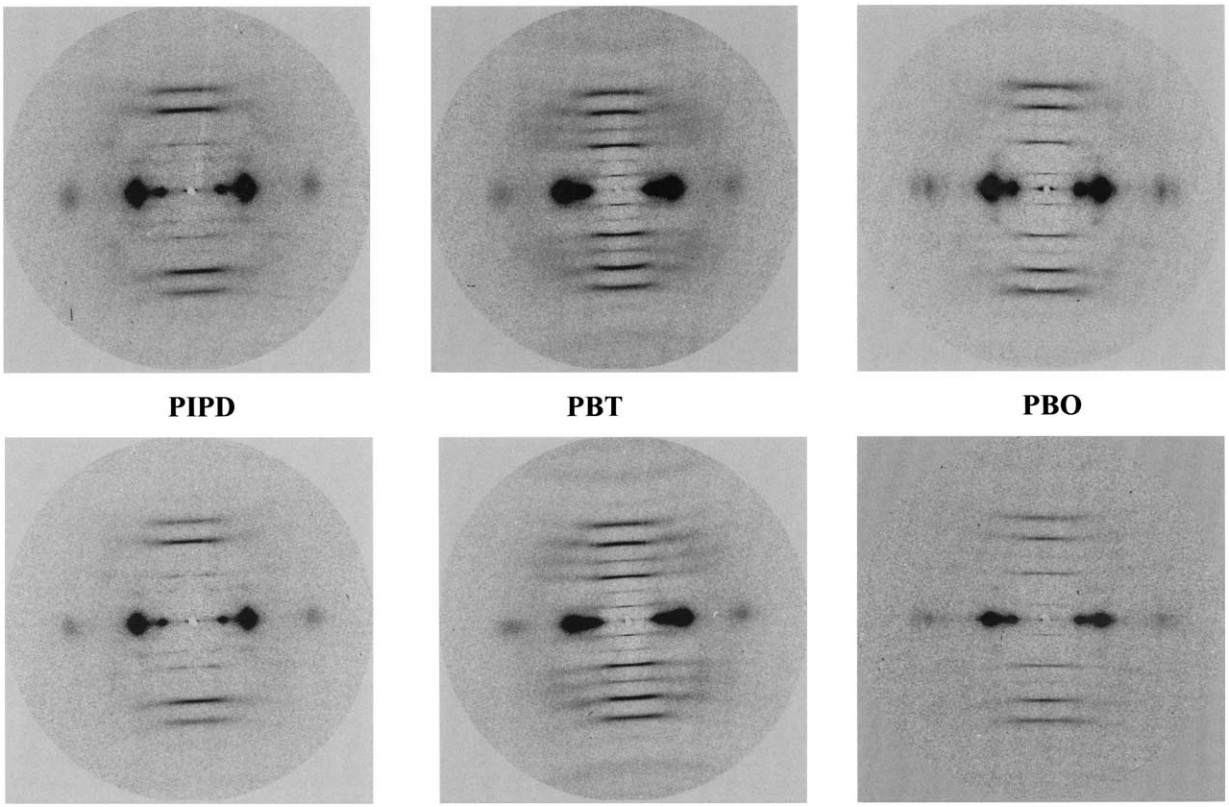

Fig. 3. Single-filament diffraction patterns of unloaded (top row) and loaded (bottom row) PIPD, PBT and PBO fibres obtained using synchrotron radiation.

view unmerged when PBT fibres are submitted to a heat-treatment under tension [23,25]. The lack of resolution of the PBT equatorial peaks with respect to those of the PBO fibre gives an indication of a poorly developed lateral order of the PBT chains in the as spun fibre. A possible explanation to this phenomenon is the non-planar configuration of the PBT molecules in PBT crystals [3], or different processing conditions to those employed in the manufacturing of PBO fibres.

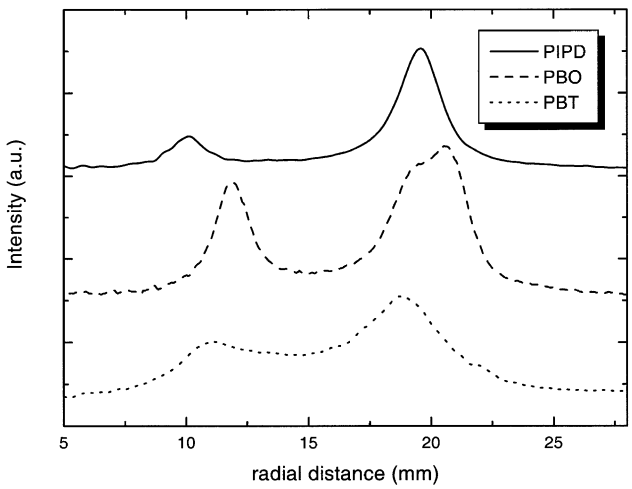

Fig. 4. Equatorial profiles of unloaded single-filament diffraction patterns (obtained using synchrotron radiation) obtained for the rigid-rod polymer-based fibres.

3.3. Crystal modulus calculation

The lower three images of Fig. 3 correspond to the diffraction patterns of the same fibres when subject to a load. Of particular interest in comparison to the loaded and unloaded diffraction patterns is the difference in definition of the equatorial peaks before and after loading of the fibres. This indicates that the orientation distribution of the crystallites within the fibre is improving during loading, a subject that will be discussed on the next paper in this series.

Macroscopic deformation of the fibres will induce changes at microscopic level, specifically interatomic distances, and hence to the deformation of the unit cell. Due to the microstructure of the rigid-rod polymer-based fibres, major changes in atomic distances of the polymer backbone are expected, since the polymeric chains align into microfibrils along the fibre axis [3]. This effect brings about a shift of the meridional reflections with external stress (Fig. 5). By measuring the amount of meridional peak movement during the loading of the fibre (Fig. 5), the change in *c*-spacing (i.e. in the direction of the fibre axis) of the unit cell can be calculated. A microscopic fibre strain can be thus estimated and used finally to determine the crystal modulus of the fibre. Fig. 6 shows the stress versus lattice strain plots and crystal modulus values for each of the three fibre types.

The first comment that must be pointed out in the discussion of the results shown in Fig. 6 is related to the

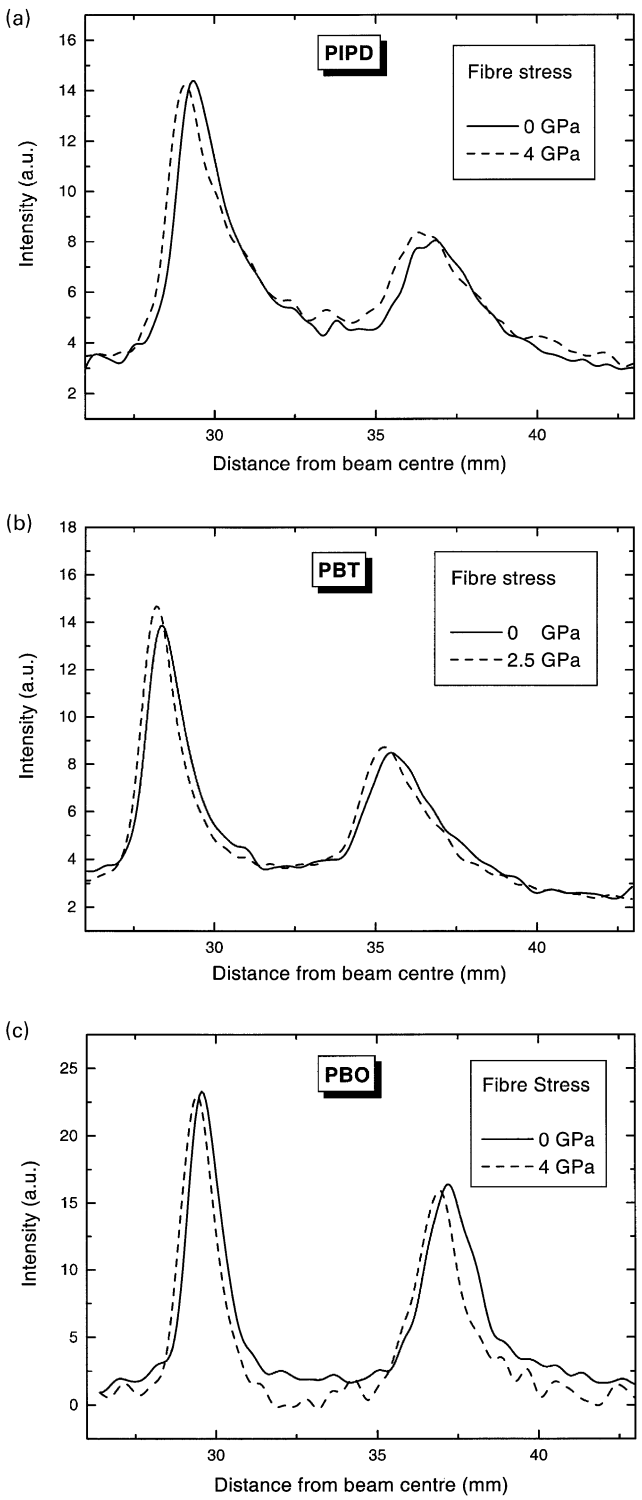

Fig. 5. Shift of the (005) and (006) Bragg reflections with stress for single (a) PIPD, (b) PBT and (c) PBO-fibres.

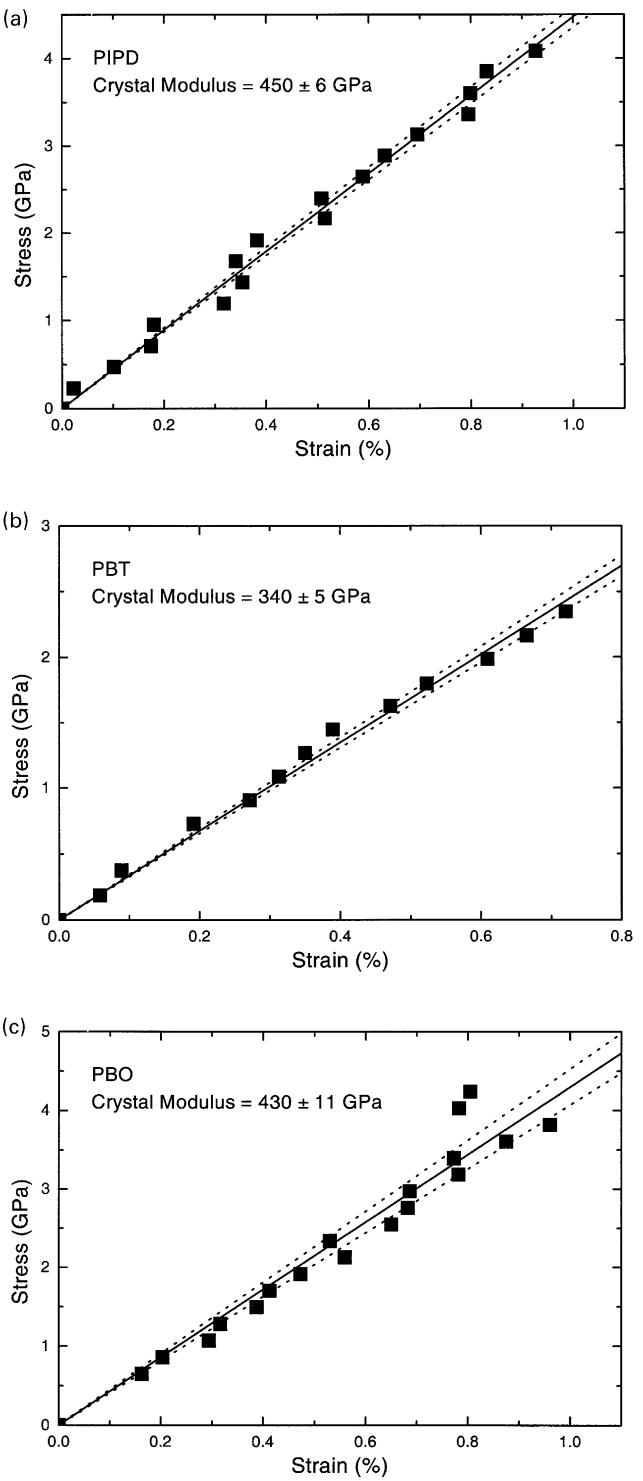

Fig. 6. Plots of stress versus lattice strain (*c*-direction) for single (a) PIPD, (b) PBT and (c) PBO fibres. The crystal modulus and 95% confidence limit bands (dotted lines) also indicated.

uncertainty of the crystal moduli values. The single-fibre diffraction technique employed in this work clearly offers a very accurate way of calculating the crystal modulus of polymeric fibres. Indeed, errors due to experimental factors are approximately 2% of the reported value, as shown by the confidence bands also drawn in Fig. 6. However, the influence of fibre diameter variation has not been included. Such variations as those shown in Table 1 could result in a systematic error greater than the experimental error, approximately 6–7% for the fibres studied here. Although the uncertainty is still acceptable, performing fibre diameter

measurements locally to experimental sites can easily eliminate this undesirable source of error.

The values of PBT and PBO crystal modulus depicted in Fig. 6 agree well, within experimental error, with results obtained by other researchers as shown in Table 1. Lenhert and Adams [11] reported values of 350 and 390 for as-spun PBT and PBO fibres, respectively. It is worth to note that these authors carried out several studies using the fibre-bundle diffraction method, where a number of filaments are deformed and an averaged cross-section is utilised. The agreement between their results [11] and those shown in this work (Fig. 6) would therefore indicate that the 'homogeneous stress' assumption (i.e. the load on the crystals is the applied load divided by the cross-sectional area of the fibres) required for fibre-bundle determination of crystal modulus is valid. The same authors found a 15–20% increase of crystal modulus in heat-treated PBT and PBO samples [11]. Whether or not there must exist such differences between the crystal moduli of treated and untreated fibres is not clear. In principle, similar moduli should be expected as both as spun and heat-treated fibres present the same crystal structure (this is not the case for PIPD fibres). This idea has been supported by crystal modulus measurements carried out more recently with PBO (430 and 460 GPa for as spun and heat-treated samples, respectively) [13], and PBT fibres (370 GPa for a heat-treated sample) [14].

Due to the novelty of the PIPD fibre, we have found only a very few results to compare with the present measurements. In fact, this is to our knowledge the first time that the crystal modulus of PIPD fibres has been measured directly by means of diffraction techniques. Lammers et al. [8] used an indirect method to estimate the crystal modulus of as spun and heat-treated fibres. They tested mechanically single filaments to determine their individual tensile modulus (E_i). For each filament, they also evaluated the crystal orientation distribution using single-fibre XRD. Plotting $1/E_i$ vs. $\langle \sin^2\phi \rangle_E$, they could estimate the crystal modulus of PIPD fibres by extrapolation at $\langle \sin^2\phi \rangle_E = 0$ (i.e. perfect crystal orientation), thus reporting values of 320 and 500 GPa for as spun and heat-treated PIPD fibres, respectively [8] (Table 1). However, these results must be taken with care, as their standard errors are quite large (60 GPa). Nevertheless, they seem to be reasonable when compared to 440 GPa obtained in the present work. On the other hand, density functional theory calculations render a higher crystal modulus (560 GPa) [26]. This discrepancy was expected to some extent since ab initio values are usually upper bounds to experimental crystal modulus.

A direct comparison of the three values (Fig. 6) shows the PBT fibre to have a crystal modulus significantly lower than that of both the PIPD and PBO fibre, which in turn is very similar. Differences found previously between PBO and PBT crystal modulus have been explained in terms of molecular geometry factors [25,27]. XRD studies have shown a non-planar geometry of the monomers in PBO and PBT fibres, as well as PIPD fibres, due to rotation of the phenylene ring about the connecting C–C bond [23]. This non-planarity is especially noticeable in the case of PBT, with an average torsion angle of 46°, whereas PBO and PIPD monomers, with torsion angles of 10 and 8°, respectively, are fairly closed to planarity [7,23]. The reason behind this difference is that PBT monomers present a considerable steric hindrance due to the bulky sulphur atoms of the bisthiazole moiety, leading to a high torsion angle to minimise the conformational energy. Theoretical calculations support partially the experimental observations. Hence, geometry optimisations following ab initio calculations on PIPD [26] and semi-empirical methods on PBO monomers [28] result in planar structures. Semi-empirical optimal molecular geometries of PBT monomers, on the other hand, are non-planar [28], although more refined ab initio calculations lead to planar geometries [29]. Nonetheless, it seems that there exists a close relationship between the torsion angle and the modulus of rigid-rod polymer crystals. This is rather expected since both the C–C bond connecting the two ring systems and the phenyl moiety suffer maximum deformation levels in the molecule, for a given stress [26]. At the same time and comparing the values of PIPD and PBO, it also seems that the inter- and intra-molecular hydrogen bonds present in the PIPD rigid-rod system do not affect the final value of the crystal modulus.

As expected, the crystal moduli of the rigid-rod polymer-based fibres (Fig. 6) are much higher than those (macroscopic) values determined from tensile experiments (Table 1). This demonstrates the effect of flaws, impurities, voids and poor crystallite orientation within the fibres, all of which lower the measured Young's modulus from its crystal modulus value. Of the three fibre varieties, the PIPD fibre has a Young's modulus much closer to the crystal modulus than the other two types of fibre, being almost the 50% compared to the 40 and 35% of the PBO and PBT fibres, respectively. This improvement in Young's modulus can be attributed to the heat-treatment of the PIPD fibre. In fact, mechanical modulus of heat-treated PBO and PBT have shown values (~300 GPa) [11] somewhat closer to the upper limit given by the crystal modulus.

4. Conclusions

High-quality XRD patterns could be obtained from single rigid-rod polymer-based fibres by means of synchrotron radiation. This allowed the study of fibre deformation avoiding the natural drawbacks appearing when fibre bundles are used (i.e. averaging stresses). Crystal modulus of PIPD, PBO and PBT were thus determined accurately, and compared to results obtained by other authors. Similar moduli were obtained for PIPD and PBO (440 GPa), whereas a lower one was calculated for PBT (350 GPa). The non-linearity of PBT monomers in the unit cell seems to

be the reason behind this difference. In comparison with tensile data, the crystal modulus of the three fibre types was found to be greater than the Young's modulus. This indicates the influence of factors reducing the measured tensile modulus of the fibres, such as flaws, voids, impurities and poor crystallite orientation. This difference was reduced significantly in the case of the PIPD fibre. This demonstrates the effectiveness of post-heat treatments in improving the mechanical properties of rigid-rod polymer-based fibres.

Acknowledgments

The authors would like to extend our thanks to EPSRC for funding this project, the ESRF for beam time, and Akzo Nobel (the Netherlands), the Air Force Materials Laboratory (USA) and Toyobo (Japan) for supplying the fibre samples. They would also like to thank Dr Andrew Hammersley for the FIT2D software application, Craig Meakin and all other colleagues in the Manchester Materials Science Centre who have collaborated with us in this work.

References

[1] Kumar S. In: Lee SM, editor. Encyclopedia of composites, vol. 14. New York: VCH; 1990.
[2] Adams WW, Eby RK, McLemore DE, editors. Mater Res Soc Symp Proc 1989;134.
[3] Jiang H, Adams WW, Eby RK. In: Lewin M, Preston J, editors. High technology fibers. Part B. New York: Marcel Dekker; 1996.
[4] Calundann G, Jaffe M, Jones RS, Yoon H. In: Bunsell AR, editor. Fibre reinforcements for composite materials. Amsterdam: Elsevier; 1988.
[5] Tomlin DW, Fratini AV, Hunsaker M, Adams WW. Polymer 2000; 41:9003.
[6] Sikkema JD. Polymer 1998;39:5981.
[7] Klop EA, Lammers M. Polymer 1998;39:5987.
[8] Lammers M, Klop EA, Northolt MG, Sikkema DJ. Polymer 1998;39: 5999.
[9] Sirichaisit J, Young RJ. Polymer 1999;40:3421.
[10] Dulmage WJ, Contois LE. J Polym Sci 1958;28:275.
[11] Lenhert PG, Adams WW. Mater Res Soc Symp Proc 1989;134:329.
[12] Kitagawa T, Ishitobi M, Yabuki K. J Polym Sci, Part B: Polym Phys 2000;38:1605.
[13] Davies RJ, Montes-Morán MA, Riekel C, Young RJ. J Mater Sci 2001;36:3079.
[14] Nakamae K, Nishino T, Gotoh Y, Matsui R, Nagura M. Polymer 1999;40:4629.
[15] Riekel C, Dieing T, Engstrom P, Vincze L, Martin C, Mahendrasingam A. Macromolecules 1999;32:7859.
[16] Riekel C, Cedola A, Heidelbach F, Wagner K. Macromolecules 1997; 30:1033.
[17] Müller M, Riekel C, Vuong R, Chanzy H. Polymer 2000;41:2627.
[18] Riekel C, Müller M, Vollrath F. Macromolecules 1999;32:4464.
[19] Hammersley AP. ESRF Internal Report, ESRF97HA02T; 1997.
[20] Hammersley AP, Riekel C. Syn Rad News 1989;2:24.
[21] Martin DC, Thomas EL. Macromolecules 1991;24:2450.
[22] Tashiro K, Yoshino J, Kitagawa T, Murase H, Yabuki K. Macromolecules 1998;31:5430.
[23] Fratini AV, Lenhert PG, Resch TJ, Adams WW. Mater Res Soc Symp Proc 1989;134:431.
[24] Northolt MG, Van Aartsen JJ. J Polym Sci Polym Symp 1997;58:283.
[25] Odell JA, Keller A, Atkins EDT, Miles MJ. J Mater Sci 1981;16:3309.
[26] Hageman JCL, van der Horst JW, Groot RA. Polymer 1999;40:1313.
[27] Krause SJ, Haddock TB, Vezie DL, Lenhert PG, Hwang W-F, Price GE, Helminiak TE, O'Brien JF, Adams WW. Polymer 1988;29:1354.
[28] Tashiro K, Kobayashi M. Macromolecules 1991;24:3706.
[29] Trohalaki S, Dudis DS. Polymer 1995;36:911.